

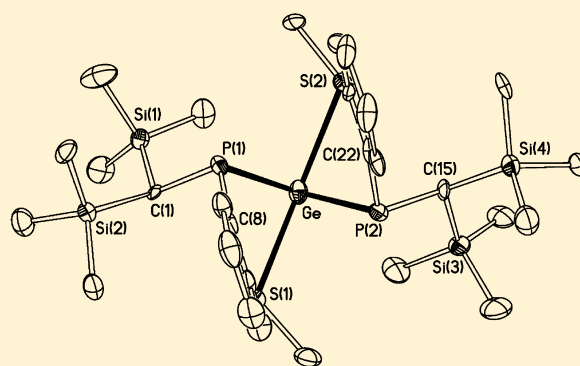
# Hypervalent Sulfur-Functionalized Diphosphagermylene and Diphosphastannylene Compounds

Keith Izod,\* Ewan R. Clark, William Clegg, and Ross W. Harrington

Main Group Chemistry Laboratories, School of Chemistry, Bedson Building, Newcastle University, Newcastle upon Tyne, NE1 7RU, U.K.

## Supporting Information

**ABSTRACT:** The reaction between either  $\text{GeCl}_2(1,4\text{-dioxane})$  or  $\text{SnCl}_2$  and 2 equiv of the lithium phosphide  $[\{(\text{Me}_3\text{Si})_2\text{CH}\}\text{P}(\text{C}_6\text{H}_4\text{-2-SMe})\}\text{Li}(\text{tmeda})]$  gives the corresponding diphosphatetrylenes  $[\{(\text{Me}_3\text{Si})_2\text{CH}\}\text{P}(\text{C}_6\text{H}_4\text{-2-SMe})\}_2\text{E}$  [ $\text{E} = \text{Ge}$  (**10**),  $\text{Sn}$  (**11**)] in good yields. Both **10** and **11** crystallize as discrete monomers in which the Ge and Sn atoms are coordinated by both P and S atoms. Although **10** and **11** crystallize as racemic mixtures of the *RR* and *SS* diastereomers, variable-temperature NMR experiments suggest that, in solution, these compounds are in dynamic equilibrium with small amounts of the corresponding *RS* and *SR* diastereomers. DFT calculations reveal that the lowest-energy minima for both **10** and **11** possess *rac* stereochemistry; two higher-energy minima were located for each of **10** and **11**, both of which have *meso* stereochemistry. The two calculated *meso* diastereomers differ in the location of the sulfur and phosphorus substituents within the pseudo-trigonal-bipyramidal structures. Both **10** and **11** decompose on exposure to light, generating the diphosphine  $\{(\text{Me}_3\text{Si})_2\text{CH}\}(\text{C}_6\text{H}_4\text{-2-SMe})\text{P-P}(\text{C}_6\text{H}_4\text{-2-SMe})\{\text{CH}(\text{SiMe}_3)_2\}$  (**14**) as the major product.



## INTRODUCTION

Over the last two decades, the chemistry of diaminocarbenes ( $\text{R}_2\text{N})_2\text{C}$  and their cyclic analogues (N-heterocyclic carbenes, NHCs) has seen a rapid and extraordinary expansion, due principally to the unique properties of these compounds and their widespread application as ligands for catalytically active transition-metal complexes.<sup>1</sup> The stability of diaminocarbenes is largely due to efficient  $p\pi-p\pi$  overlap of the nitrogen lone pairs with the vacant p orbital at carbon, which mitigates the electron deficiency of this center and which results in these compounds having good  $\sigma$ -donor, but poor  $\pi$ -acceptor, ligand characteristics.

While the first stable diaminocarbenes were reported in the early 1990s, the heavier group 14 analogues of these compounds, the diaminetetrylenes,  $(\text{R}_2\text{N})_2\text{E}$  ( $\text{E} = \text{Ge}, \text{Sn}, \text{Pb}$ ), have been known for some time.<sup>2</sup> This is principally due to the increasing stability of the +2 oxidation state with increasing atomic number, and the ready availability of  $\text{Ge}(\text{II}), \text{Sn}(\text{II}),$  and  $\text{Pb}(\text{II})$  precursors. However, despite this, there are surprisingly few examples of stable diphosphacarbenes,  $(\text{R}_2\text{P})_2\text{C}$ , and diphosphatetrylenes,  $(\text{R}_2\text{P})_2\text{E}$ . This may be attributed to the large barrier to inversion at phosphorus, which inhibits planarization at the phosphorus center, a key requirement for effective  $p\pi-p\pi$  overlap of the phosphorus lone pair with the vacant p orbital at the group 14 element center.<sup>3,4</sup> Nonetheless, a small number of diphosphatetrylenes and related species have been reported,<sup>5–10</sup> including both monomeric species, such as  $\{(\text{Tripp})_2\text{FSi}\}(i\text{Pr}_3\text{Si})\text{P}\}_2\text{E}$  [ $\text{E} = \text{Ge}, \text{Sn}, \text{Pb}; \text{Tripp} = 2,4,6-$

$i\text{Pr}_3\text{C}_6\text{H}_2$ ],<sup>5</sup> and dimeric species, such as  $\{(t\text{Bu}_2\text{P})_2\text{Pb}\}_2$ ,<sup>6</sup>  $\{(\text{Me}_3\text{Si})_2\text{P}\}_2\text{Pb}$ ,<sup>7</sup> and  $\{(i\text{Pr}_2\text{P})_2\text{Ge}\}_2$ ,<sup>8</sup> several ate complexes and mixed group 2/group 14 phosphide and phosphinidene complexes have also been reported.<sup>11–13</sup> In addition, Bertrand and co-workers have shown that, under very specific conditions, stable P-heterocyclic carbenes are accessible, in which the phosphorus atoms adjacent to the carbene center approach planarity.<sup>14</sup>

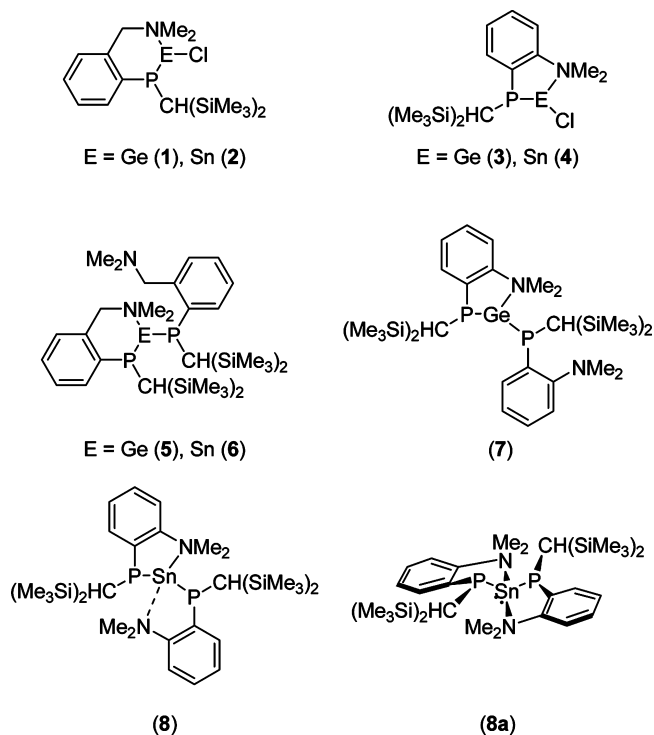
We have recently reported a series of intramolecularly base-stabilized mono- and diphosphatetrylenes (**1–8**, Chart 1).<sup>15–18</sup> The structures and dynamic behavior of these compounds are significantly affected by the nature of the group 14 center and the size of the potential chelate ring. In the solid state, the diphosphagermylenes **5** and **7** crystallize as monomers in which one phosphide ligand chelates the germanium center, while the other acts as a terminal P-donor ligand; in both structures, the second amino substituent is oriented away from the germanium center.<sup>15,17</sup> A similar situation prevails for the tin analogue **6**, which has one chelating and one terminal phosphide ligand;<sup>16</sup> however, **8** (the tin analogue of **7**) crystallizes with a somewhat different structure in which the second amino substituent forms a relatively close contact with the tin center ( $\text{Sn-P}, 3.306(3) \text{ \AA}$ ).<sup>17</sup>

In solution, the diphosphagermylenes **5** and **7** are subject to dynamic equilibria that (i) interconvert the chelating and

Received: September 5, 2011

Published: December 7, 2011

Chart 1



terminal phosphide ligands and (ii) interconvert diastereomers via inversion at the phosphorus and/or germanium centers.<sup>15,17</sup>

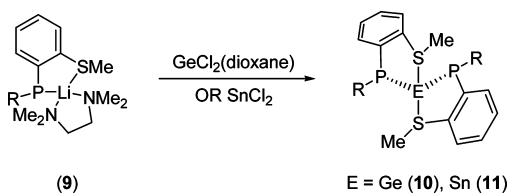
For 5 and 7, both of these processes may be observed by variable-temperature NMR spectroscopy. For 6, epimerization appears to be rapid on the NMR time scale and only interconversion of the chelating and terminal phosphide ligands is observed.<sup>16</sup> For 8, a different situation prevails: at high temperatures, both epimerization and chelating-terminal ligand exchange are rapid, whereas at low temperatures, a single pseudo-trigonal-bipyramidal species is observed in which both amino groups are bound to the tin center (8a).<sup>17</sup>

We now report the synthesis of a new diphosphagermylene and diphosphastannylene and show that incorporation of a soft sulfur-donor functionality into the phosphide ligand favors the formation of four-coordinate pseudo-trigonal-bipyramidal structures for these species.

## RESULTS AND DISCUSSION

**Synthesis.** The reaction between 2 equiv of the lithium phosphide  $[\{(Me_3Si)_2CH\}P(C_6H_4-2-SMe)]Li(tmeda)$  (**9**)<sup>19</sup> and either  $GeCl_2(1,4\text{-dioxane})$  or  $SnCl_2$  in THF, in the absence of light, gives the corresponding diphosphatetrylenes  $[\{(Me_3Si)_2CH\}P(C_6H_4-2-SMe)]_2E$  [ $E = \text{Ge (10), Sn (11)}$ ] as orange, air-sensitive solids in 64 and 90% yield, respectively (Scheme 1). The exclusion of light during these reactions is

Scheme 1.  $R = CH(SiMe_3)_2$



imperative as this prevents isomerization of the lithium salt **9** to the corresponding thiolate  $[\{(Me_3Si)_2CH\}P(Me)(C_6H_4-2-S)]Li(tmeda)$  (see below).<sup>19</sup> Compounds **10** and **11** are highly soluble, even in hydrocarbon solvents, but were crystallized as orange blocks suitable for X-ray crystallography from cold hexamethyldisiloxane containing a few drops of diethyl ether. Both **10** and **11** crystallize under these conditions as diethyl ether solvates, although the two compounds differ in the proportion of solvent incorporated: thus, **10** crystallizes as the hemisolvate  $[\{(Me_3Si)_2CH\}P(C_6H_4-2-SMe)]_2Ge \cdot 1/2Et_2O$  (**10a**), whereas **11** crystallizes as the monosolvate  $[\{(Me_3Si)_2CH\}P(C_6H_4-2-SMe)]_2Sn \cdot Et_2O$  (**11a**). For **11a**, the solvent of crystallization is only weakly held and is rapidly lost under vacuum; <sup>1</sup>H NMR spectra and elemental analyses of **11a** reveal substoichiometric quantities of diethyl ether to be present after exposure of the crystalline material to vacuum for a few minutes. The solvent of crystallization in **10a** appears to be more tightly held and is not lost on exposure to vacuum for short periods.

We have previously reported the straightforward synthesis of the heteroleptic compounds **1–4** from the reaction between either  $GeCl_2(1,4\text{-dioxane})$  or  $SnCl_2$  and the corresponding lithium or potassium phosphide.<sup>15–17</sup> Somewhat surprisingly, attempts to prepare the corresponding heteroleptic, thioether-functionalized compounds  $[\{(Me_3Si)_2CH\}P(C_6H_4-2-SMe)]ECl$  ( $E = \text{Ge, Sn}$ ) were unsuccessful. The reaction between **9** and 1 equiv of  $GeCl_2(1,4\text{-dioxane})$  yields only the homoleptic compound **10**, as judged by <sup>1</sup>H and <sup>31</sup>P{<sup>1</sup>H} NMR spectroscopy, and half an equivalent of the known adduct  $GeCl_2(tmeda)$  (the identity of this latter compound was confirmed by X-ray crystallography).<sup>20</sup> The corresponding reaction between **9** and 1 equiv of  $SnCl_2$  similarly yields **11** as the only phosphorus-containing product, which was crystallized from *n*-hexane as the solvate  $[\{(Me_3Si)_2CH\}P(C_6H_4-2-SMe)]_2Sn \cdot 1/2C_6H_{14}$  (**11b**), as confirmed by X-ray crystallography (see the Supporting Information). In an attempt to rule out the intermediacy of *tmeda* in the formation of **10** and **11**, we prepared the 12-crown-4 adduct of **9**,  $[\{(Me_3Si)_2CH\}P(C_6H_4-2-SMe)]Li(12\text{-crown-4})$  (**9a**) as a potential starting material; however, the reaction between **9a** and 1 equiv of  $SnCl_2$  again yields the homoleptic compound **11**. A small number of colorless crystals, which were isolated from this reaction, were shown by X-ray crystallography to be the trichlorostannate complex  $[Li(12\text{-crown-4})(THF)][SnCl_3]$  (**12**) (see the Supporting Information). The isolation of **10–12** from these reactions suggests that ligand exchange is rapid under the conditions employed and that there is a strong preference for the formation of the homoleptic diphosphatetrylenes. This is in marked contrast to the behavior of related amino-functionalized ligands, where the heteroleptic species **1–4** are readily isolated. The isolation of the homoleptic compounds in these reactions may be attributed to the softer nature and reduced steric demands of the SMe groups in **10** and **11**, compared with the hard, more sterically demanding  $NMe_2$  groups in **1–8**.

**Solid-State Structures.** The structures of **10a** and **11a** are shown in Figure 1, along with selected bond lengths and angles. Both **10a** and **11a** crystallize as discrete molecular species in which the group 14 centers are four-coordinate, bound by the P and S atoms of two chelating phosphide ligands [bite angles: **10a**, 76.11(5)° and 75.41(5)°; **11a**, 72.47(5)° and 72.97(5)°]. This affords a pseudo-trigonal-bipyramidal geometry at the group 14 element center in each case, with the sterically

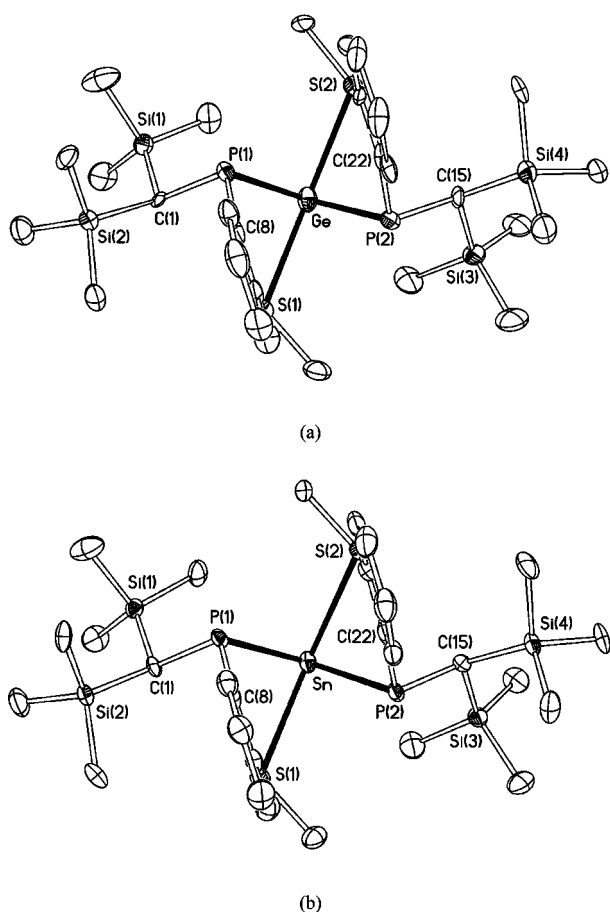


**Figure 1.** Molecular structures of (a) **10a** and (b) **11a** with 40% probability ellipsoids; H atoms and solvent of crystallization omitted for clarity. Selected bond lengths (Å) and angles (deg). For **10a**: Ge–P(1) 2.4302(16), Ge–P(2) 2.4327(14), Ge–S(1) 2.7793(15), Ge–S(2) 2.8220(15), P(1)–Ge–S(1) 76.11(5), P(2)–Ge–S(2) 75.41(5), S(1)–Ge–S(2) 148.26(4), P(1)–Ge–P(2) 100.63(5). For **11a**: Sn–P(1) 2.6080(17), Sn–P(2) 2.6087(17), Sn–S(1) 2.9404(17), Sn–S(2) 2.9055(17), P(1)–Sn–S(1) 72.47(5), P(2)–Sn–S(2) 72.97(5), S(1)–Sn–S(2) 140.66(5), P(1)–Sn–P(2) 100.71(5).

hindered phosphorus atoms in the equatorial positions, as expected. Because of the constraints associated with the formation of the two chelate rings and the larger size of tin compared with that of germanium, the S(1)–Sn–S(2) angle in **11a** [140.66(5)°] is smaller than the S(1)–Ge–S(2) angle in **10a** [148.26(4)°], and both are significantly distorted away from the ideal 180°. Compounds **10a** and **11a** are chiral at both of the phosphorus centers, and both compounds crystallize as a racemic mixture of the  $P_RP_R$  and  $P_S P_S$  diastereomers.

The Ge–P distances of 2.4302(16) and 2.4327(14) Å in **10a** are similar to the few previously reported Ge(II)–P distances; for example, the Ge–P distances in dimeric [(*i*-Pr<sub>2</sub>P)<sub>2</sub>Ge]<sub>2</sub> are 2.4261(11), 2.4217(11), and 2.3981(11) Å,<sup>8</sup> whereas the Ge–P distance in [CH{(CMe)(2,6-*i*-Pr<sub>2</sub>C<sub>6</sub>H<sub>3</sub>N)}<sub>2</sub>Ge{P(SiMe<sub>3</sub>)<sub>2</sub>} is 2.3912(8) Å.<sup>9</sup> Similarly, the Sn–P distances in **11a** [2.6080(17) and 2.6087(17) Å] are comparable to those in **6** [2.5906(9) and 2.6407(8) Å]<sup>16</sup> and **8** [2.5995(10) and 2.6110(11) Å].<sup>17</sup> Few Ge(II)–S distances have been reported, and none between a Ge(II) center and a thioether; however, the Ge–S distances [2.7793(15) and 2.8220(15) Å] are, as expected, somewhat longer than the few reported Ge–S distances in Ge(II) thiolates, such as {(Me<sub>3</sub>Si)<sub>3</sub>C}Ge(μ-SBu)<sub>2</sub>Li(THF)<sub>2</sub> [Ge–S,

2.393(2) and 2.386(2) Å].<sup>21</sup> Similarly, there are no previous reports of crystallographically characterized compounds in which a Sn(II) center is bound by a thioether. The Sn–S distances of 2.9055(17) and 2.9404(17) Å are rather long; for example, the Sn–S distances in trimeric (DippS)Sn(μ-DippS)<sub>2</sub>Sn(μ-DippS)<sub>2</sub>Sn(DippS) range from 2.471(5) to 2.838(4) Å,<sup>22</sup> whereas the corresponding distances in {(Me<sub>3</sub>Si)<sub>3</sub>C}Sn(μ-S-*t*-Bu)<sub>2</sub>Li(THF)<sub>2</sub> are 2.568(1) and 2.574(1) Å [Dipp = 2,6-Pr<sup>*t*</sup><sub>2</sub>C<sub>6</sub>H<sub>3</sub>].<sup>21</sup>

**Solution-State Behavior.** Our previous variable-temperature and multielement NMR spectroscopic studies have shown that the amino-functionalized diphosphagermylene **7** is subject to dynamic equilibria in solution.<sup>17</sup> The low-temperature <sup>31</sup>P{<sup>1</sup>H} NMR spectrum of **7** exhibits signals due to three of the four possible diastereomers, whereas at room temperature and above, a single set of ligand signals is observed in both the <sup>31</sup>P{<sup>1</sup>H} and the <sup>1</sup>H NMR spectra due to rapid exchange between diastereomers and between the chelating and terminal phosphide ligands. The solution behavior of **8** is somewhat different: while at room temperature, **8** appears to be subject to similar dynamic equilibria to those observed for **7**, interconversion between diastereomers appears to be more rapid than exchange between the chelating and terminal phosphide ligands, and exchange between diastereomers may not be frozen out. At –80 °C, the <sup>31</sup>P{<sup>1</sup>H}, <sup>1</sup>H, and <sup>119</sup>Sn NMR spectra of **8** are consistent with the predominance of a single pseudo-trigonal-bipyramidal species (**8a**).<sup>17</sup>

The <sup>31</sup>P{<sup>1</sup>H} NMR spectra of **10** and **11** exhibit somewhat different characteristics to those of both **7** and **8**. At room temperature, the <sup>31</sup>P{<sup>1</sup>H} NMR spectrum of **10** in *d*<sub>8</sub>-toluene exhibits a single, slightly broadened singlet at –26.6 ppm. As the temperature is reduced, this signal broadens significantly and moves to higher field, until, at –30 °C, the spectrum consists of a broad singlet at –28.0 ppm. Below this temperature, this signal sharpens again, until, at –60 °C, the spectrum consists of a single, reasonably sharp singlet at –28.3 ppm.

At –60 °C, the <sup>1</sup>H NMR spectrum of **10** in *d*<sub>8</sub>-toluene is entirely consistent with the structure observed crystallographically: a single set of ligand signals is observed, in which the diastereotopic SiMe<sub>3</sub> groups give rise to distinct singlets at –0.09 and –0.36 ppm. As the temperature is increased, the SiMe<sub>3</sub> signals coalesce to give a single peak, such that, at room temperature, these protons give rise to a single, relatively sharp singlet at 0.09 ppm. Similarly, the well-resolved set of aromatic signals observed at –60 °C broadens with increasing temperature, before sharpening to a new set of signals at room temperature. Perhaps most notably, at –60 °C, the Si<sub>2</sub>CHP group gives rise to a somewhat broad singlet at 1.93 ppm (A), which broadens substantially and moves upfield as the temperature is increased, until, at –30 °C, this group gives rise to a broad singlet at 1.76 ppm (Figure 2). Above this temperature, this signal continues to move upfield, but now sharpens, until, at room temperature, the Si<sub>2</sub>CHP group gives rise to a relatively sharp singlet at 1.48 ppm. The line shape of the signal due to the SMe protons (B) does not change significantly as the temperature is increased from –60 °C, but this signal shifts from 2.04 ppm at this temperature to 2.18 ppm at room temperature.

The variable-temperature NMR spectra of **11** exhibit similar characteristics to those of **10**. The room-temperature <sup>31</sup>P{<sup>1</sup>H} NMR spectrum of **11** in *d*<sub>8</sub>-toluene consists of a sharp singlet at –34.7 ppm, exhibiting satellites due to coupling to <sup>117/119</sup>Sn

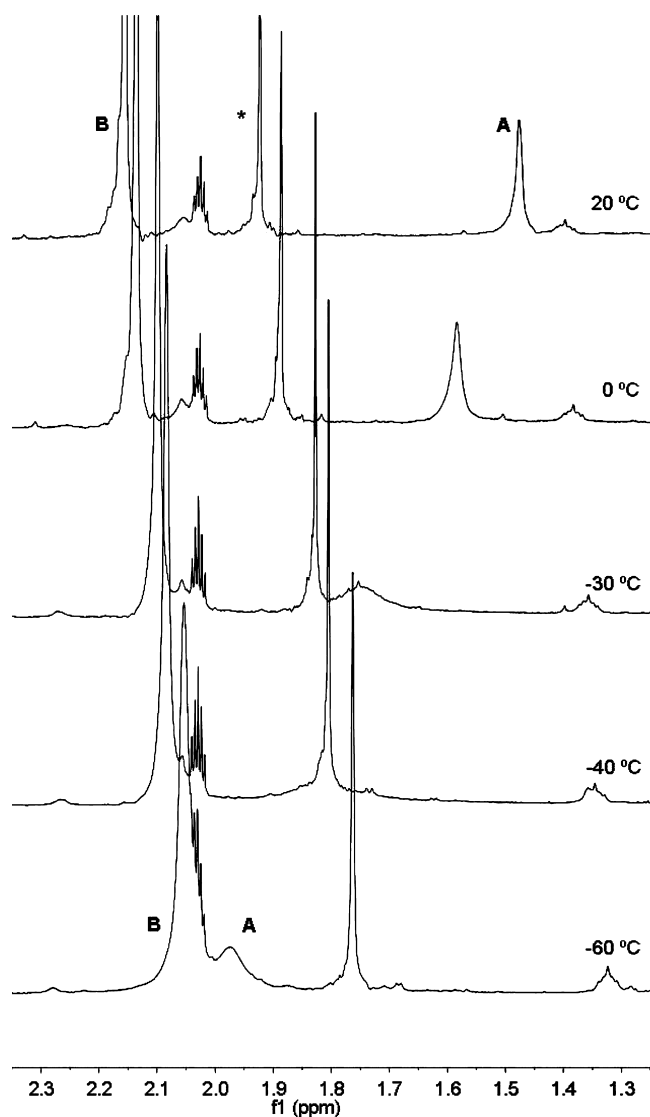


**Figure 2.** Expansion of the variable-temperature  $^1\text{H}$  NMR spectra of **10** in  $d_8$ -toluene, showing the CHP region [\* free phosphine  $\{(\text{Me}_3\text{Si})_2\text{CH}\}\text{PH}(\text{C}_6\text{H}_4\text{-}2\text{-SMe})$  due to a small amount of hydrolysis during sample preparation].

( $J_{\text{SnP}} = 1027$  and  $1072$  Hz). This signal shifts to slightly higher field as the temperature is reduced, with only a marginal change to its line width; the  $^{31}\text{P}\{^1\text{H}\}$  NMR spectrum of **11** at  $-70$  °C consists of a sharp singlet at  $-38.2$  ppm, exhibiting poorly resolved  $^{117}/^{119}\text{Sn}$  satellites ( $J_{\text{SnP}} = 1062$  Hz). The variable-temperature  $^1\text{H}$  NMR spectra of **11** follow a similar pattern to those of **10**. The diastereotopic  $\text{SiMe}_3$  groups give rise to two sharp singlets at  $-0.04$  and  $0.39$  ppm at  $-60$  °C, which coalesce to a single broad singlet at  $0.06$  ppm at room temperature. The signal due to the  $\text{Si}_2\text{CHP}$  group shifts from approximately  $2.07$  ppm at  $-60$  °C (this signal is obscured by that due to the  $\text{SMe}$  protons at this temperature) to  $1.86$  ppm at room temperature, without any significant change to its line shape. At the same time, the signal due to the  $\text{SMe}$  protons shifts from  $2.07$  ppm at  $-60$  °C to  $2.17$  ppm at room temperature. We were unable to locate a  $^{119}\text{Sn}$  signal at room temperature, probably as a consequence of rapid dynamic exchange (see below); however, at  $-60$  °C, a binomial triplet is observed at  $657$  ppm ( $J_{\text{SnP}} = 1072$  Hz).

The low-temperature NMR spectra of both **10** and **11** are consistent with the presence of a single, symmetrical species in each case, with a structure corresponding to that observed crystallographically. At higher temperatures, both compounds appear to be subject to dynamic equilibria between the dominant *rac* diastereomer observed at low temperatures and the corresponding *meso* diastereomer, the latter of which is present only in very low concentrations; thus, at room temperature, a time-averaged  $^1\text{H}$  NMR spectrum is observed in which the diastereotopic  $\text{SiMe}_3$  groups give rise to a single peak.

The unusually low-field shifts of the  $\text{Si}_2\text{CHP}$  methine protons in the low-temperature  $^1\text{H}$  NMR spectra of both **10** and **11** may be attributed to the proximity of these protons to the lone pairs at the sulfur and germanium/tin centers in the *rac* diastereomer. In contrast, DFT calculations suggest that in neither of the two *meso* diastereomer conformations located, are both of the methine protons in such a position (see below). The unusual temperature-dependent behavior of the chemical shift of the  $\text{Si}_2\text{CHP}$  protons in **10** and **11** may, therefore, be attributed to a dynamic equilibrium between the *rac* and *meso* diastereomers in each case. At low temperatures, the *rac* diastereomer predominates and a low-field  $\text{Si}_2\text{CHP}$  shift is observed. However, as the temperature is raised, the proportion of the *meso* diastereomer increases, and so a time-averaged signal is observed for these protons, which moves to higher field as the proportion of *meso* diastereomer increases.

**DFT Calculations.** To gain further insight into the relative stabilities of the two diastereomers of **10** and **11**, we have undertaken a DFT study of these compounds. The ground-state geometries of the complete molecules were optimized using the hybrid B3LYP functional,<sup>23</sup> with a Lanl2dz effective core potential basis set on tin<sup>24</sup> and a 6-31G(d,p) basis set on all other atoms;<sup>25</sup> the location of minima was confirmed by the absence of imaginary vibrational frequencies.

For each compound, three distinct minima were located (Figure 3). The lowest-energy minima located in each case (**10**<sub>1</sub> and **11**<sub>1</sub>) correlate extremely well with the structures obtained by X-ray crystallography; details of selected bond lengths and angles for all minima located are given in Table 1. In both **10**<sub>1</sub> and **11**<sub>1</sub>, the germanium and tin atoms adopt a pseudo-trigonal-bipyramidal structure in which the sterically less hindered, more electronegative sulfur substituents lie in the axial positions. The calculated Ge–P and Sn–P distances [ $2.4325$  and  $2.6320$  Å, respectively] in both **10**<sub>1</sub> and **11**<sub>1</sub> are slightly longer than those observed crystallographically [Ge–P,  $2.4302(16)$  and  $2.4327(14)$  Å; Sn–P,  $2.6080(17)$  and  $2.6087(17)$  Å], while there is a more significant difference between the calculated Ge–S and Sn–S distances [ $2.8593$  and  $3.0504$  Å, respectively] compared with the corresponding distances in **10a** [ $2.7793(15)$  and  $2.8220(15)$  Å] and **11a** [ $2.9055(17)$  and  $2.9404(17)$  Å]. There is a good correspondence between the calculated and crystallographically determined angles about the Ge and Sn centers. That the lowest-energy diastereomer for both **10** and **11** has a *rac* configuration is consistent with both the crystal structures of **10a** and **11a** and the variable-temperature  $^1\text{H}$  and  $^{31}\text{P}\{^1\text{H}\}$  NMR spectra of these compounds, which indicate that *rac*-**10** and *rac*-**11** predominate at low temperatures.

Two distinct minima were located for the *meso* diastereomers of both **10** and **11**. Minima **10**<sub>2</sub> and **11**<sub>2</sub> possess pseudo-trigonal-bipyramidal geometries at the germanium and tin centers, respectively, in which the sulfur substituents occupy the axial positions, as expected. The bond lengths and angles in **10**<sub>2</sub>

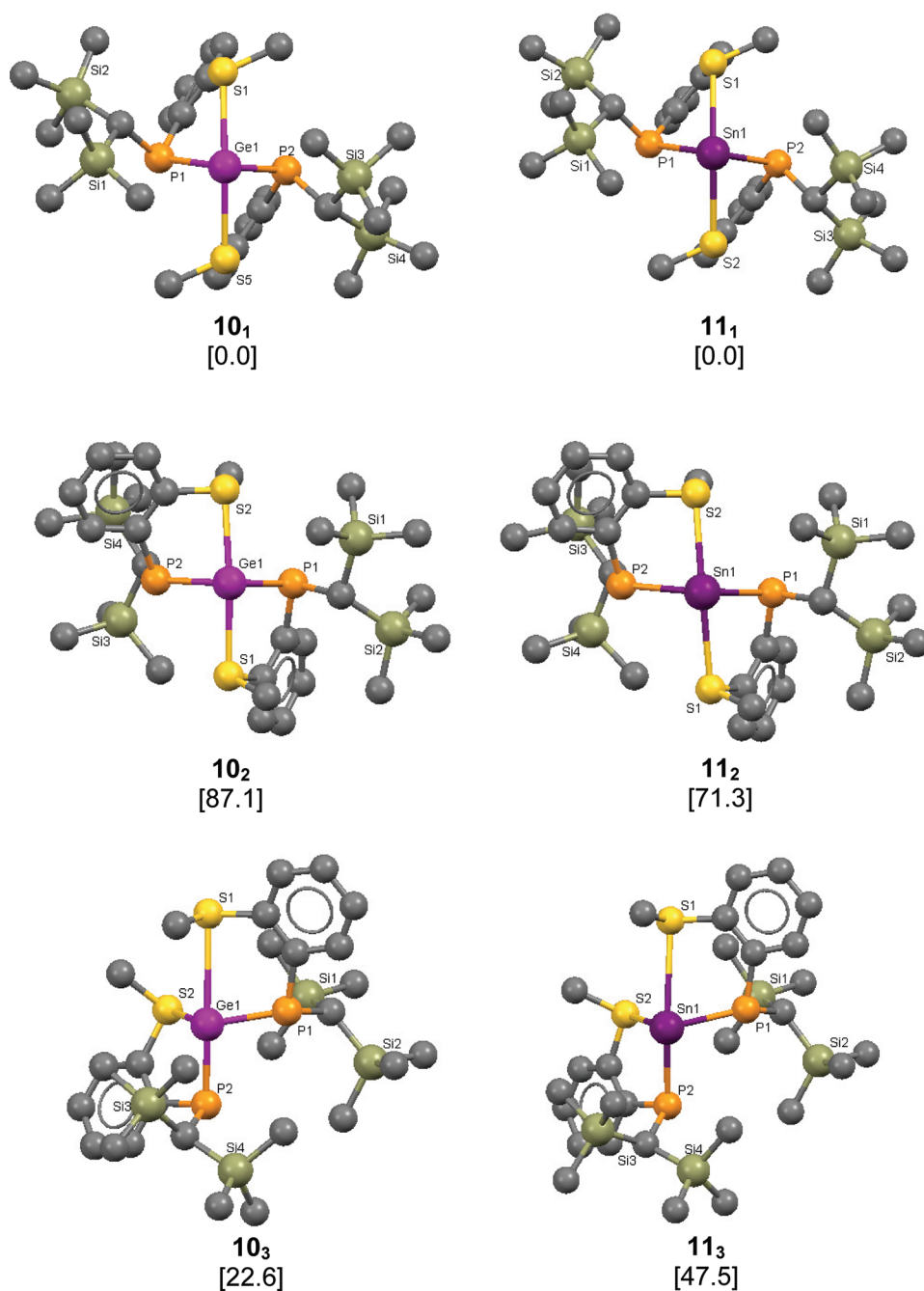


**Figure 3.** Calculated minimum-energy geometries for **10** and **11** with H atoms omitted for clarity; energies ( $\text{kJ mol}^{-1}$ ) relative to the ground states in square brackets [B3LYP/6-31G(d,p), Lanl2dz(Sn)].

**Table 1.** Selected Bond Lengths ( $\text{\AA}$ ) and Angles (deg) for the Calculated Minimum-Energy Geometries **10**<sub>1</sub>, **10**<sub>2</sub>, **10**<sub>3</sub>, and **11**<sub>1</sub>, **11**<sub>2</sub>, **11**<sub>3</sub>, and for Crystallographically Characterized **10a** and **11a**

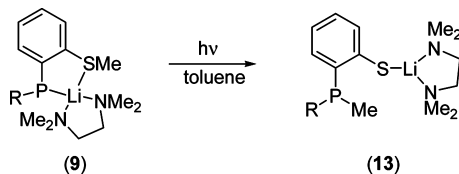
	E = Ge				E = Sn			
	<b>10a</b>	<b>10<sub>1</sub></b>	<b>10<sub>2</sub></b>	<b>10<sub>3</sub></b>	<b>11a</b>	<b>11<sub>1</sub></b>	<b>11<sub>2</sub></b>	<b>11<sub>3</sub></b>
E–P(1)	2.4302(16)	2.4325	2.4147	2.3773	2.6080(17)	2.6320	2.6856	2.5710
E–P(2)	2.4327(14)	2.4325	2.4675	2.4542	2.6087(17)	2.6320	2.6821	2.6697
E–S(1)	2.7793(15)	2.8593	2.7487	3.2632	2.9055(17)	3.0504	2.9525	3.3839
E–S(2)	2.8220(15)	2.8593	2.7504	2.5706	2.9404(17)	3.0503	2.9573	2.8293
S(1)–E–S(2)	148.26(4)	154.20	168.54	84.03	140.66(5)	142.35	160.83	77.70
P(1)–E–P(2)	100.63(5)	102.13	111.77	100.52	100.71(5)	101.31	113.76	98.58
P(1)–E–S(1)	76.11(5)	77.09	84.73	79.78	72.47(5)	71.21	78.47	74.38
P(2)–E–S(2)	75.41(5)	77.09	84.09	85.13	72.97(5)	71.21	78.53	78.04

and **11**<sub>2</sub> are similar to those in **10**<sub>1</sub> and **11**<sub>1</sub>, although the E–S distances are somewhat shorter and the P–E–S, S–E–S, and P–E–P angles are somewhat larger in **10**<sub>2</sub> and **11**<sub>2</sub> than in the ground-state geometries. Somewhat unexpectedly, we also located a second minimum-energy geometry for the *meso* diastereomers. The germanium and tin atoms in **10**<sub>3</sub> and **11**<sub>3</sub> again adopt a pseudo-trigonal-bipyramidal geometry; however, in each case, one of the sulfur substituents lies in an equatorial position, while one of the sterically bulky phosphorus substituents lies in an axial position. As expected, the axial Ge–P and Sn–P distances [2.4542 and 2.6697 Å, respectively] in **10**<sub>3</sub> and **11**<sub>3</sub> are significantly longer than the equatorial Ge–P and Sn–P distances [2.3773 and 2.5710 Å, respectively], although these distances are not significantly longer than the equatorial Ge–P and Sn–P distances in **10**<sub>2</sub> and **11**<sub>2</sub>. More strikingly, while the equatorial Ge–S and Sn–S distances [2.5706 and 2.8293 Å, respectively] are significantly shorter than the axial Ge–S and Sn–S distances in **10**<sub>2</sub> and **11**<sub>2</sub>, the axial Ge–S and Sn–S distances [3.2632 and 3.3839 Å, respectively] are extremely long, suggesting only very weak E⋯S interactions in these cases. In this regard, the structure of **11**<sub>3</sub> closely resembles the X-ray crystal structure of the amino-substituted analogue **8**, in which there is one strong and one weak Sn–N contact [Sn–N(1), 2.408(3) Å; Sn⋯N(2), 3.306(3) Å].

Perhaps surprisingly, given the above, the relative energies of **10**<sub>3</sub> and **11**<sub>3</sub> [22.7 and 47.5 kJ mol<sup>−1</sup>, respectively] are substantially lower than those of **10**<sub>2</sub> and **11**<sub>2</sub> [87.1 and 71.3 kJ mol<sup>−1</sup>, respectively], despite the positioning of one of the bulky phosphorus substituents in an equatorial site in the former geometries. This is likely a reflection of the ability of the bulky CH(SiMe<sub>3</sub>)<sub>2</sub> group to orientate itself in such a way as to minimize steric interactions and of the somewhat similar electronegativities of S and P (Pauling electronegativities of 2.19 and 2.55, respectively).

**Photolysis of 10 and 11.** We previously reported that the lithium phosphide **9** is subject to a photolytically induced isomerization to the corresponding thiolate [ $\{(\text{Me}_3\text{Si})_2\text{CH}\}\text{P}(\text{Me})(\text{C}_6\text{H}_4\text{-}2\text{-S})\}\text{Li}(\text{tmeda})$ ] (**13**) (Scheme 2).

Scheme 2



We were interested to observe whether a similar phosphide-thiolate isomerization would occur when the phosphorus center was coordinated to a softer germanium(II) or tin(II) center rather than a hard lithium cation. In the absence of air and light, compounds **10** and **11** appear to be stable for long periods; however, exposure of solutions of **10** in toluene to ambient light for 3 days leads to slow isomerization. <sup>31</sup>P{<sup>1</sup>H} NMR spectra of the crude photolyzed solutions indicate the presence of several species; significant intensity peaks were observed at −18.7, −25.7, −39.5, and −57.0 ppm. The presence of multiple species suggests that the photolysis of **10** is not straightforward; in contrast, the photolysis of the lithium complex **9** proceeds cleanly to give the thiolate **13** as the sole phosphorus-containing product. The difference in behavior between **9** and

**10** on photolysis may, at least partly, be attributed to the presence of two adjacent phosphide ligands in the latter, compared to a single ligand in the former compound. Thus, intramolecular migration of a methyl group within a ligand is favored for **9**, whereas for **10**, alternative decomposition pathways are available. Consistent with this, a major component of the photolysis products of **10** is the diphosphine  $\{(\text{Me}_3\text{Si})_2\text{CH}\}(\text{C}_6\text{H}_4\text{-}2\text{-SMe})\text{P-P}(\text{C}_6\text{H}_4\text{-}2\text{-SMe})\{\text{CH}(\text{SiMe}_3)_2\}$  (**14**), formed via a reductive elimination process, presumably generating elemental germanium as a side product; compound **14** gives rise to the signal at −18.7 ppm in the <sup>31</sup>P{<sup>1</sup>H} NMR spectrum of the photolysis products of **10** (see below for further details of the characterization of this compound). In addition, it is possible for migration of the S-methyl group to occur either from the sulfur atom to the phosphorus atom within one ligand or from the sulfur atom of one ligand to the phosphorus atom of an adjacent ligand; in either case, this will potentially lead to the formation of more than one diastereomer and thus a rather complex <sup>31</sup>P{<sup>1</sup>H} NMR spectrum.

Exposure of solutions of the diphosphastannylene **11** in toluene to ambient light for 1 day leads to the deposition of elemental tin and the formation of the diphosphine **14** as the sole phosphorus-containing product, suggesting that reductive elimination is more rapid than ligand isomerization for this compound. The <sup>31</sup>P{<sup>1</sup>H} NMR spectrum of **14** formed under these conditions exhibits a dominant peak at −18.2 ppm along with a much lower intensity signal at −24.8 ppm; the ratio of these peaks is approximately 15:1, suggesting that **14** is formed predominantly as a single diastereomer.

The identity of **14** was confirmed by X-ray crystallography. Although both our DFT studies and our variable-temperature NMR data suggest that the *rac* diastereomer of **11** predominates and so that the dominant product of reductive elimination of **11** should be *rac*-**14**, the crystal of **14** studied by crystallography was found to be of the *meso* diastereomer. The molecular structure of *meso*-**14** is shown in Figure 4, along with selected bond lengths and angles.

Compound *meso*-**14** crystallizes in an approximately antiperiplanar conformation with a dihedral angle of 179° between the nominal lone-pair directions. The P–P distance of 2.2278(12) Å is similar to the corresponding distance in the related diphosphine  $\{(\text{Me}_3\text{Si})_2\text{CH}\}(\text{C}_6\text{H}_4\text{-}2\text{-CH}_2\text{NMe}_2)\text{P-P}(\text{C}_6\text{H}_4\text{-}2\text{-CH}_2\text{NMe}_2)\{\text{CH}(\text{SiMe}_3)_2\}$  [2.2304(6) Å]<sup>26</sup> and in other diphosphine compounds.<sup>27</sup> The two ends of the diphosphine adopt significantly different conformations, such that the mean plane of the aromatic ring bound to P(2) lies almost in the same plane as the P(1)–P(2) axis, whereas the aromatic ring bound to P(2) lies nearly perpendicular to this axis.

## CONCLUSIONS

A small change in the nature of the peripheral donor functionality in the ligands [ $\{(\text{Me}_3\text{Si})_2\text{CH}\}\text{P}(\text{C}_6\text{H}_4\text{-}2\text{-X})\}$ ]<sup>−</sup> (from X = NMe<sub>2</sub> to SMe) has significant consequences for the structure and dynamic behavior of the corresponding diphosphatetrylenes  $\{[\{(\text{Me}_3\text{Si})_2\text{CH}\}\text{P}(\text{C}_6\text{H}_4\text{-}2\text{-X})]_2\text{E}$  [X = NMe<sub>2</sub>, E = Ge (**7**), Sn (**8**); X = SMe, E = Ge (**10**), Sn (**11**)]. In both **7** and **8**, the tetrel atom adopts a trigonal-pyramidal configuration, bound by the two phosphorus atoms and one of the nitrogen atoms of the ligands, although **8** exhibits a weak Sn⋯N contact to the second nitrogen atom in the molecule. In contrast, in compounds **10** and **11**, the better

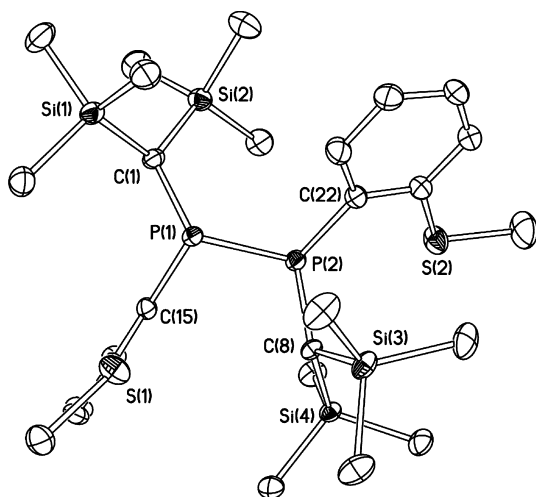


**Figure 4.** Molecular structure of *meso*-14, with 40% probability ellipsoids and with H atoms omitted for clarity. Selected bond lengths (Å) and angles (deg): P(1)–P(2) 2.2278(12), P(1)–C(1) 1.882(3), P(1)–C(15) 1.853(3), P(2)–C(8) 1.871(3), P(2)–C(22) 1.848(3), C(1)–P(1)–C(15) 100.55(15), C(1)–P(1)–P(2) 109.21(11), C(15)–P(1)–P(2) 94.54(11), C(8)–P(2)–C(22) 106.85(15), C(8)–P(2)–P(1) 97.33(11), C(22)–P(2)–P(1) 100.95(11).

match between the soft sulfur donor and the relatively soft Ge(II) and Sn(II) centers leads to stronger E–S interactions, resulting in pseudo-trigonal-bipyramidal geometry at the tetrel centers. DFT calculations indicate that the *rac* diastereomers of **10** and **11**, as observed in the solid state, are significantly more stable than the corresponding *meso* diastereomers. However, variable-temperature  $^1\text{H}$  and  $^{31}\text{P}\{^1\text{H}\}$  NMR spectroscopies suggest that, in solution, while *rac*-**10** and *rac*-**11** predominate at low temperatures, these species are in dynamic equilibrium with the corresponding *meso* diastereomers at higher temperatures.

## EXPERIMENTAL SECTION

All manipulations were carried out using standard Schlenk techniques under an atmosphere of dry nitrogen. Diethyl ether, THF, light petroleum (bp 40–60 °C), *n*-hexane, and toluene were dried prior to use by distillation under nitrogen from sodium, potassium, or sodium/potassium alloy; hexamethyldisiloxane was purified by distillation under nitrogen from CaH<sub>2</sub>. THF and hexamethyldisiloxane were stored over activated 4A molecular sieves; all other solvents were stored over a potassium film. Deuterated toluene was distilled from potassium and deoxygenated by three freeze–pump–thaw cycles and was stored over activated 4A molecular sieves.  $[\{(\text{Me}_3\text{Si})_2\text{CH}\}P(\text{C}_6\text{H}_4\text{-}2\text{-SMe})]\text{Li}(\text{tmeda})$  was prepared by a previously published procedure;<sup>19</sup> *n*-butyllithium was purchased from Aldrich as a 2.5 M solution in hexanes. All other compounds were used as supplied by the manufacturer.

$^1\text{H}$  and  $^{13}\text{C}\{^1\text{H}\}$  NMR spectra were recorded on a JEOL ECS500 spectrometer operating at 500.16 and 125.65 MHz, respectively, or a Bruker Avance300 spectrometer operating at 300.15 and 75.47 MHz, respectively; chemical shifts are quoted in parts per million relative to tetramethylsilane.  $^{31}\text{P}\{^1\text{H}\}$  and  $^{119}\text{Sn}$  NMR spectra were recorded on a JEOL ECS500 spectrometer operating at 202.35 and 186.51 MHz, respectively; chemical shifts are quoted in parts per million relative to external 85% H<sub>3</sub>PO<sub>4</sub> and Me<sub>4</sub>Sn, respectively. Elemental analyses were obtained by the Elemental Analysis Service of London Metropolitan University.

**$[\{(\text{Me}_3\text{Si})_2\text{CH}\}P(\text{C}_6\text{H}_4\text{-}2\text{-SMe})]_2\text{Ge}$  (**10**).** A solution of  $[\{(\text{Me}_3\text{Si})_2\text{CH}\}P(\text{C}_6\text{H}_4\text{-}2\text{-SMe})]\text{Li}(\text{tmeda})$  (2.02 g, 4.63 mmol) in THF (20 mL) was added dropwise to a cold (–78 °C), stirred solution of GeCl<sub>2</sub>·dioxane (0.54 g, 2.31 mmol) in THF (15 mL) in the

absence of light, over 40 min. The reaction was allowed to attain room temperature and was stirred overnight, and then solvent was removed in vacuo to give a sticky yellow solid, which was extracted into light petroleum (3 × 15 mL) and filtered. The solvent was removed in vacuo from the filtrate to give a sticky yellow solid. Single crystals of the diethyl ether solvate  $[\{(\text{Me}_3\text{Si})_2\text{CH}\}P(\text{C}_6\text{H}_4\text{-}2\text{-SMe})]_2\text{Ge}\cdot 1/2\text{Et}_2\text{O}$  (**10a**) suitable for X-ray crystallography were grown from cold (–20 °C) hexamethyldisiloxane containing a few drops of diethyl ether. Yield: 1.03 g, 63.7%. Anal. Calcd for C<sub>28</sub>H<sub>52</sub>GeP<sub>2</sub>S<sub>2</sub>Si<sub>4</sub>·1/2C<sub>4</sub>H<sub>10</sub>O: C, 48.9; H, 7.8. Found: C, 49.0; H, 7.8.  $^1\text{H}$  NMR (*d*<sub>8</sub>-toluene, 293 K): δ 0.09 (s, 36H, SiMe<sub>3</sub>), 1.05 (t, *J* = 7.1 Hz, 3H, Et<sub>2</sub>O), 1.93 (s br, 2H, CHP), 2.18 (s, 6H, SMe), 3.21 (q, *J* = 7.1 Hz, 2H, Et<sub>2</sub>O), 6.61–6.88 (m, 8H, ArH).  $^{13}\text{C}\{^1\text{H}\}$  NMR (C<sub>6</sub>D<sub>6</sub>, 293 K): δ 2.67 (SiMe<sub>3</sub>), 8.57 (d, *J*<sub>PC</sub> = 57.8 Hz, CHP), 15.80 (Et<sub>2</sub>O), 18.13 (d, *J*<sub>PC</sub> = 12.6 Hz, SMe), 67.57 (Et<sub>2</sub>O), 124.48 (d, *J*<sub>PC</sub> = 10.1 Hz, Ar), 127.17, 125.36 (Ar), 136.00 (d, *J*<sub>CP</sub> = 31.4 Hz, Ar), 144.71, 145.44 (d, *J*<sub>PC</sub> = 45.3 Hz, Ar).  $^{31}\text{P}\{^1\text{H}\}$  NMR (*d*<sub>8</sub>-toluene, 293 K): δ –26.6 (br s).

**$[\{(\text{Me}_3\text{Si})_2\text{CH}\}P(\text{C}_6\text{H}_4\text{-}2\text{-SMe})]_2\text{Sn}$  (**11**).** A solution of  $[\{(\text{Me}_3\text{Si})_2\text{CH}\}P(\text{C}_6\text{H}_4\text{-}2\text{-SMe})]\text{Li}(\text{tmeda})$  (0.83 g, 1.90 mmol) in THF (10 mL) was added, dropwise, over half an hour, to a cold (–78 °C), stirred solution of SnCl<sub>2</sub> (0.18 g, 0.95 mmol) in THF (15 mL) in the absence of light. The reaction was allowed to attain room temperature and was stirred overnight, and then solvent was removed in vacuo. The resulting orange solid was extracted into light petroleum (3 × 15 mL) and filtered, and the solvent was removed in vacuo from the filtrate to give **11** as a sticky orange solid. Single crystals of the diethyl ether solvate  $[\{(\text{Me}_3\text{Si})_2\text{CH}\}P(\text{C}_6\text{H}_4\text{-}2\text{-SMe})]_2\text{Sn}\cdot\text{Et}_2\text{O}$  (**11a**) suitable for X-ray crystallography were obtained from cold (–30 °C) hexamethyldisiloxane containing a few drops of diethyl ether. Yield: 0.64 g, 90.3%. Anal. Calcd for C<sub>28</sub>H<sub>52</sub>P<sub>2</sub>S<sub>2</sub>Si<sub>4</sub>Sn: C, 45.1; H, 7.0%. Found: C, 45.7; H, 7.1%.  $^1\text{H}$  NMR (*d*<sub>8</sub>-toluene, 293 K): δ 0.06 (s, 36H, SiMe<sub>3</sub>), 1.05 (t, *J* = 7.1 Hz, 2H, Et<sub>2</sub>O), 1.86 (s, 2H, CHP), 2.17 (s, 6H, SMe), 3.20 (q, *J* = 7.1 Hz, 3H, Et<sub>2</sub>O), 6.57–6.77 (m, 8H, ArH).  $^{13}\text{C}\{^1\text{H}\}$  NMR (*d*<sub>8</sub>-toluene, 293 K): δ 2.37 (SiMe<sub>3</sub>), 6.61 (d, *J*<sub>PC</sub> = 61.4 Hz, CHP), 15.26 (Et<sub>2</sub>O), 16.92 (d, *J*<sub>PC</sub> = 13.4 Hz, SMe), 65.60 (Et<sub>2</sub>O), 124.37, 127.11 (Ar), 138.33 (d, *J*<sub>PC</sub> = 42.2 Hz, Ar), 144.72 (d, *J*<sub>PC</sub> = 49.9 Hz, Ar), 146.49 (Ar).  $^{31}\text{P}\{^1\text{H}\}$  NMR (*d*<sub>8</sub>-toluene, 293 K): δ –34.7 (s, *J*<sub>SnP</sub> = 1072 and 1027 Hz).  $^{119}\text{Sn}$  NMR (*d*<sub>8</sub>-toluene, 237 K): δ 657 (t, *J*<sub>SnP</sub> = 1072 Hz).

**Attempted Synthesis of  $[\{(\text{Me}_3\text{Si})_2\text{CH}\}P(\text{C}_6\text{H}_4\text{-}2\text{-SMe})]\text{GeCl}$ .** A solution of  $[\{(\text{Me}_3\text{Si})_2\text{CH}\}P(\text{C}_6\text{H}_4\text{-}2\text{-SMe})]\text{Li}(\text{tmeda})$  (0.485 g, 1.11 mmol) in THF (10 mL) was added dropwise to a cold (–78 °C), stirred solution of GeCl<sub>2</sub>·dioxane (0.257 g, 1.11 mmol) in THF (10 mL) over 20 min in the absence of light. The stirred reaction mixture was allowed to attain room temperature overnight, yielding a yellow solution. The solvent was removed in vacuo to give a sticky yellow solid. The product was extracted into light petroleum (2 × 10 mL) and filtered, and solvent was removed in vacuo from the filtrate to give a yellow solid, which was shown by  $^1\text{H}$  and  $^{31}\text{P}\{^1\text{H}\}$  NMR spectroscopies to be the homoleptic compound **10a**.

This reaction was repeated under similar conditions. However, in this instance, the sticky yellow solid was extracted into diethyl ether, rather than light petroleum, and the ether extract was cooled to –20 °C, leading to the deposition of a small number of colorless crystals, which were shown by X-ray crystallography to be the known adduct GeCl<sub>2</sub>·TMEDA.

### Attempted Synthesis of $[\{(\text{Me}_3\text{Si})_2\text{CH}\}P(\text{C}_6\text{H}_4\text{-}2\text{-SMe})]\text{SnCl}$ .

**Route 1.** To a stirred, cold (–78 °C) solution of SnCl<sub>2</sub> (0.278 g, 1.47 mmol) in THF (15 mL) was added a solution of  $[\{(\text{Me}_3\text{Si})_2\text{CH}\}P(\text{C}_6\text{H}_4\text{-}2\text{-SMe})]\text{Li}(\text{tmeda})$  (0.640 g, 1.47 mmol) in THF (10 mL), and the reaction mixture was allowed to attain room temperature overnight. The solvent was removed in vacuo, the product was extracted into diethyl ether (3 × 15 mL) and filtered, and solvent was removed in vacuo from the filtrate to give a yellow solid, which was shown by  $^1\text{H}$  and  $^{31}\text{P}\{^1\text{H}\}$  NMR spectroscopies to be the homoleptic compound **11**. An alternative batch of single crystals of **11** suitable for X-ray crystallography was grown from cold (–20 °C) *n*-hexane and found to be the *n*-hexane solvate  $[\{(\text{Me}_3\text{Si})_2\text{CH}\}P(\text{C}_6\text{H}_4\text{-}2\text{-SMe})]_2\text{Sn}\cdot 1/2\text{C}_6\text{H}_{14}$  (**11b**).

Table 2. Crystallographic Data for 10a, 11a, 11b, 12, and 14

compound	10a	11a	11b	12	14
formula	C <sub>28</sub> H <sub>52</sub> GeP <sub>2</sub> S <sub>2</sub> Si <sub>4</sub> ·0.5C <sub>4</sub> H <sub>10</sub> O	C <sub>28</sub> H <sub>52</sub> P <sub>2</sub> S <sub>2</sub> Si <sub>4</sub> Sn·C <sub>4</sub> H <sub>10</sub> O	C <sub>28</sub> H <sub>52</sub> P <sub>2</sub> S <sub>2</sub> Si <sub>4</sub> Sn·0.5C <sub>6</sub> H <sub>14</sub>	C <sub>12</sub> H <sub>24</sub> LiO <sub>5</sub> <sup>+</sup> SnCl <sub>3</sub> <sup>-</sup>	C <sub>28</sub> H <sub>52</sub> P <sub>2</sub> S <sub>2</sub> Si <sub>4</sub>
M <sub>w</sub>	736.8	819.9	788.9	480.3	627.1
cryst size (mm)	0.12 × 0.10 × 0.10	0.20 × 0.10 × 0.10	0.24 × 0.10 × 0.10	0.40 × 0.20 × 0.01	0.40 × 0.30 × 0.30
cryst syst	monoclinic	monoclinic	monoclinic	monoclinic	monoclinic
space group	C2/c	P2 <sub>1</sub> /c	P2 <sub>1</sub> /c	P2 <sub>1</sub> /n	P2 <sub>1</sub> /c
a (Å)	30.494(2)	16.9798(15)	10.4746(2)	9.6864(4)	19.6717(7)
b (Å)	11.1789(7)	11.0771(10)	21.3062(4)	8.3921(3)	11.3658(4)
c (Å)	22.9459(14)	23.0424(18)	18.4807(3)	23.1898(12)	15.8141(5)
β (deg)	91.760(5)	99.466(8)	102.3116(19)	94.973(4)	91.836(3)
V (Å <sup>3</sup> )	7818.3(9)	4275.0(6)	4029.56(13)	1877.98(14)	3534.0(2)
Z	8	4	4	4	4
μ (mm <sup>-1</sup> )	1.115	0.905	0.956	1.802	0.394
trans coeff range	0.878–0.897	0.840–0.915	0.803–0.911	0.533–0.840	0.858–0.891
reflins measd	18342	25684	38038	10803	17814
unique reflins	6872	8243	10038	4509	5060
R <sub>int</sub>	0.121	0.058	0.032	0.021	0.026
reflins with F <sup>2</sup> > 2σ	3160	5104	7460	3578	4561
parameters	371	395	377	199	339
R (on F, F <sup>2</sup> > 2σ) <sup>a</sup>	0.061	0.060	0.023	0.023	0.048
R <sub>w</sub> (on F <sup>2</sup> , all data) <sup>a</sup>	0.068	0.169	0.050	0.056	0.120
goodness of fit <sup>a</sup>	0.955	0.997	0.902	1.020	1.061
max, min electron density (e Å <sup>-3</sup> )	0.72, -0.71	3.25, -0.95	0.37, -0.43	0.52, -0.50	1.58, -0.34

<sup>a</sup>Conventional  $R = \sum |F_o| - |F_c| / \sum |F_o|$ ;  $R_w = [\sum w(F_o^2 - F_c^2)^2 / \sum w(F_o^2)^2]^{1/2}$ ;  $S = [\sum w(F_o^2 - F_c^2)^2 / (\text{no. data} - \text{no. params})]^{1/2}$  for all data.

**Route 2.** In the absence of light, [ $\{(Me_3Si)_2CH\}P(C_6H_4-2-SMe)Li(tmeda)$ ] (1.20 g, 2.75 mmol) was dissolved in hot light petroleum (50 mL), and the solution was cooled to room temperature. One equivalent of 12-crown-4 (0.44 mL, 0.48 g, 2.75 mmol) was added to this solution, with immediate formation of a dark red solid, and this mixture was stirred for 1 h. The supernatant was decanted and the sticky solid washed with light petroleum (20 mL). The resulting red solid was dissolved in THF (20 mL) and filtered to remove a pale, insoluble precipitate and the solvent once more removed to give crude [ $\{(Me_3Si)_2CH\}P(C_6H_4-2-SMe)Li(12-crown-4)$ ] (1.04 g, 2.09 mmol). The crown ether complex was dissolved in THF (25 mL) and added dropwise to a cold (-78 °C), stirred solution of SnCl<sub>2</sub> (0.397 g, 2.09 mmol) in THF (25 mL). The reaction was stirred overnight and allowed to attain room temperature, giving a very pale yellow solution. Solvent was removed in vacuo to give a pale paste that was extracted into diethyl ether (2 × 20 mL); the combined extracts were filtered and solvent was removed in vacuo from the filtrate to give a sticky, cream solid. The solid was dissolved in diethyl ether (10 mL), filtered, and stored at -20 °C, whereupon a small number of colorless single crystals deposited, which were shown by X-ray crystallography to be the trichlorostannate complex [Li(12-crown-4)(THF)][SnCl<sub>3</sub>] (12).

**Photolysis of 11 and Isolation of [ $\{(Me_3Si)_2CH\}P(C_6H_4-2-SMe)_2$ ] (14).** Compound 11 (0.14 g, 0.19 mmol) was dissolved in toluene (20 mL) under nitrogen in a standard borosilicate glass Schlenk tube and exposed to direct sunlight. After 16 h of continuous exposure, the solvent was removed in vacuo, giving a thick, greasy solid that was extracted with hot light petroleum (2 × 20 mL). The combined extracts were filtered to remove the dark solids, and solvent was removed in vacuo from the filtrate to afford 14 as a waxy yellow solid. The product was recrystallized from cold (-20 °C) *n*-hexane as colorless blocks suitable for X-ray crystallography. Yield: 0.17 g, 89.5%. <sup>1</sup>H NMR (CDCl<sub>3</sub>, 293 K): δ -0.06 (s, 18H, SiMe<sub>3</sub>), 0.00 (s, 18H, SiMe<sub>3</sub>), 2.46 (d, J<sub>PH</sub> = 12.4 Hz, 2H, CHP), 2.48 (s, 6H, SMe), 7.19–7.13 (m, 4H, ArH), 7.35 (m, 2H, ArH), 8.08 (m, 2H, ArH). <sup>13</sup>C{<sup>1</sup>H} NMR (CDCl<sub>3</sub>, 293 K): δ 2.58 (t, J<sub>PC</sub> = 5.3 Hz, SiMe<sub>3</sub>), 2.74 (s, SiMe<sub>3</sub>), 9.65 (t, J<sub>PC</sub> = 23.0 Hz, CHP), 16.06 (t, J<sub>PC</sub> = 7.2 Hz, SMe), 124.00, 129.69 (Ar), 136.66 (t, J<sub>PC</sub> = 7.7 Hz, ArH), 147.08 (t, J<sub>PC</sub> = 17.3 Hz, ArH). <sup>31</sup>P{<sup>1</sup>H} NMR (CDCl<sub>3</sub>, 293 K): δ -18.2.

**Crystal Structure Determinations of 10a, 11a, 11b, 12, and 14.** Measurements were made at 150 K on an Oxford Diffraction (now Agilent Technologies) Gemini A Ultra diffractometer using graphite-monochromated Mo Kα radiation (λ = 0.71073 Å) and ω scans. Cell parameters were refined from the observed positions of all strong reflections. Intensities were corrected semiempirically for absorption, based on symmetry-equivalent and repeated reflections. The structures were solved by direct methods and refined on F<sup>2</sup> values for all unique data. Table 2 gives further details. All non-hydrogen atoms were refined anisotropically, and H atoms were constrained with a riding model. U(H) was set at 1.2 (1.5 for methyl groups) times U<sub>eq</sub> for the parent atom. Programs were Oxford Diffraction CrysAlisPro and SHELXTL for structure solution, refinement, and molecular graphics.<sup>28</sup> Although disorder is likely for the ether molecule lying on a 2-fold rotation axis in 10a, this could not be resolved satisfactorily, and the geometry was restrained on the basis of well-ordered molecules found in a search of the Cambridge Structural Database.<sup>29</sup> The highest difference density peaks found at the end of refinement of 11a lie close to the Sn atom and indicate imperfect absorption corrections.

**DFT Calculations.** Geometry optimizations were performed on the gas-phase molecules with the Gaussian 03 suite of programs (revision D.01)<sup>30</sup> on a 224-core Silicon Graphics Altix 4700, with 1.6 GHz Montecito Itanium2 processors, via the EPSRC National Service for Computational Chemistry Software (<http://www.nscs.ac.uk>).

Ground-state optimizations were carried out using the B3LYP hybrid functional<sup>24</sup> with an LanL2dz effective core potential basis set for Sn,<sup>25</sup> and a 6-31G(d,p) all-electron basis set on all other atoms<sup>26</sup> (default parameters were used throughout). Minima were confirmed by the absence of imaginary vibrational frequencies.

## ■ ASSOCIATED CONTENT

### Supporting Information

For 10a, 11a, 11b, 12, and 14, details of structure determination, atomic coordinates, bond lengths and angles, and displacement parameters in CIF format; for 11b and 12, structural diagrams and selected bond lengths and angles. For 10 and 11, details of DFT calculations, final atomic coordinates,

and energies. This material is available free of charge via the Internet at <http://pubs.acs.org>.

## AUTHOR INFORMATION

### Corresponding Author

\*E-mail: [k.j.izod@ncl.ac.uk](mailto:k.j.izod@ncl.ac.uk)

## ACKNOWLEDGMENTS

The authors are grateful to the EPSRC for support and acknowledge the use of the EPSRC UK National Service for Computational Chemistry Software (NSCCS) at Imperial College London in carrying out this work.

## REFERENCES

- (1) For recent reviews of N-heterocyclic carbenes and their applications, see: (a) de Fremont, P.; Marion, N.; Nolan, S. P. *Coord. Chem. Rev.* **2009**, *253*, 862. (b) Diez-Gonzalez, S.; Marion, N.; Nolan, S. P. *Chem. Rev.* **2009**, *109*, 3612. (c) Vignolle, J.; Cattoen, X.; Bourissou, D. *Chem. Rev.* **2009**, *109*, 3333. (d) Moore, J. L.; Tomislav, R. *Top. Curr. Chem.* **2010**, *291*, 77. (e) Mercks, L.; Albrecht, M. *Chem. Soc. Rev.* **2010**, *39*, 1903. (f) Nolan, S. P. *Acc. Chem. Res.* **2011**, *44*, 91.
- (2) For selected references to diamidotetrylenes, see: (a) Driess, M.; Yao, S.; Brym, M.; van Wullen, C.; Lentz, D. *J. Am. Chem. Soc.* **2006**, *128*, 9628. (b) Driess, M.; Yao, S.; Brym, M.; van Wullen, C. *Angew. Chem., Int. Ed.* **2006**, *45*, 4349. (c) Hill, N. J.; Moser, D. F.; Guzei, I. A.; West, R. *Organometallics* **2005**, *24*, 3346. (d) Fjeldberg, T.; Hope, H.; Lappert, M. F.; Power, P. P.; Thorne, A. J. *J. Chem. Soc., Chem. Commun.* **1983**, 639. (e) Olmstead, M. M.; Power, P. P. *Inorg. Chem.* **1984**, *23*, 413. (f) Tang, Y.; Felix, A. M.; Zakharov, L. N.; Rheingold, A. L.; Kemp, R. A. *Inorg. Chem.* **2004**, *43*, 7239. (g) Avent, A. G.; Drost, C.; Gehrus, B.; Hitchcock, P. B.; Lappert, M. F. *Z. Anorg. Allg. Chem.* **2004**, *630*, 2090. (h) Gans-Eichler, T.; Gudat, D.; Nieger, M. *Angew. Chem., Int. Ed.* **2002**, *41*, 1888. (i) Chorley, R. W.; Hitchcock, P. B.; Lappert, M. F.; Leung, W.-P.; Power, P. P.; Olmstead, M. M. *Inorg. Chim. Acta* **1992**, *198*, 203. (j) Braunschweig, H.; Hitchcock, P. B.; Lappert, M. F.; Pierssens, L. J.-M. *Angew. Chem., Int. Ed. Engl.* **1994**, *33*, 1156. (k) Lappert, M. F.; Slade, M. J.; Atwood, J. L.; Zaworotko, M. J. *J. Chem. Soc., Chem. Commun.* **1980**, 621. (l) Bazinet, P.; Yap, G. P. A.; Richeson, D. S. *J. Am. Chem. Soc.* **2001**, *123*, 11162. (m) Mansell, S. M.; Russell, C. A.; Wass, D. F. *Inorg. Chem.* **2008**, *47*, 11367. (n) Zabula, A. V.; Hahn, F. E.; Pape, T.; Hepp, A. *Organometallics* **2007**, *26*, 1972. (o) Hahn, F. E.; Wittenbecher, L.; LeVan, D.; Zabula, A. V. *Inorg. Chem.* **2007**, *46*, 7662. (p) Zabula, A. V.; Pape, T.; Hepp, A.; Hahn, F. E. *Organometallics* **2008**, *27*, 2756. (q) Hahn, F. E.; Zabula, A. V.; Pape, T.; Hepp, A.; Tonner, R.; Haunschild, R.; Frenking, G. *Chem.—Eur. J.* **2008**, *14*, 10716. (r) Hahn, F. E.; Heitmann, D.; Pape, T. *Eur. J. Inorg. Chem.* **2008**, 1039. (s) Charmant, J. H.; Haddow, M. F.; Hahn, F. E.; Heitmann, D.; Frölich, R.; Mansell, S. M.; Russell, C. A.; Wass, D. F. *Dalton Trans.* **2008**, 6055.
- (3) Kapp, J.; Schade, C.; El-Nahasa, A. M.; Schleyer, P.; von, R. *Angew. Chem., Int. Ed. Engl.* **1996**, *35*, 2236.
- (4) For selected studies of the inversion behavior of pyramidal phosphorus centers, see: (a) Pelzer, S.; Wichmann, K.; Wesendrup, R.; Schwerdtfeger, P. *J. Phys. Chem. A* **2002**, *106*, 6387. (b) Beachler, R. D.; Mislow, K. *J. Am. Chem. Soc.* **1970**, *92*, 4758. (c) Beachler, R. D.; Mislow, K. *J. Am. Chem. Soc.* **1971**, *93*, 773. (d) Beachler, R. D.; Casey, J. P.; Cook, R. J.; Senkler, G. H. Jr.; Mislow, K. *J. Am. Chem. Soc.* **1972**, *94*, 2859. (e) Beachler, R. D.; Andose, J. D.; Stackhouse, J.; Mislow, K. *J. Am. Chem. Soc.* **1972**, *94*, 8060. (f) Driess, M.; Merz, K.; Monsé, C. *Z. Anorg. Allg. Chem.* **2000**, *626*, 2264. (g) Dixon, D. A.; Arduengo, A. J. III; Fukunaga, T. *J. Am. Chem. Soc.* **1986**, *108*, 2461. (h) Dixon, D. A.; Arduengo, A. J. III; Roe, D. C. *J. Am. Chem. Soc.* **1986**, *108*, 6821. (i) Dixon, D. A.; Arduengo, A. J. III *J. Am. Chem. Soc.* **1987**, *109*, 338. (j) Arduengo, A. J. III; Stewart, C. A.; Davidson, F.; Dixon, D. A.; Becker, J. Y.; Cullley, S. A.; Mizen, M. B. *J. Am. Chem. Soc.* **1987**, *109*, 627. (k) Dixon, D. A.; Arduengo, A. J. III *J. Chem. Soc., Chem. Commun.* **1987**, 498. (l) Schwerdtfeger, P.; Boyd, P. D. W.; Fischer, T.; Hunt, P.; Liddell, M. *J. Am. Chem. Soc.* **1994**, *116*, 9620. (m) Edgecombe, K. E. *J. Mol. Struct. (THEOCHEM)* **1991**, *226*, 157. (n) Creve, S.; Nguyen, M. N. *J. Phys. Chem. A* **1998**, *102*, 6549. (o) Moc, J.; Morokuma, K. *Inorg. Chem.* **1994**, *33*, 551. (p) Creve, S.; Nguyen, M. N. *Chem. Phys. Lett.* **1997**, *273*, 199. (q) Minyaev, R. M.; Wales, D. J.; Walsh, T. R. *J. Phys. Chem. A* **1997**, *101*, 1384. (r) Schwerdtfeger, P.; Hunt, P. *Adv. Mol. Struct. Res.* **1999**, *5*, 223. (s) Göller, A.; Clark, T. *Chem. Commun.* **1997**, 1033. (t) Izod, K.; Clark, E. R.; Stewart, J. *Inorg. Chem.* **2011**, *50*, 3651.
- (5) Driess, M.; Janoschek, R.; Pritzkow, H.; Rell, S.; Winkler, U. *Angew. Chem., Int. Ed.* **1995**, *34*, 1614.
- (6) Cowley, A. H.; Giolando, D. M.; Jones, R. A.; Nunn, C. M.; Power, J. M. *Polyhedron* **1988**, *7*, 1909.
- (7) Goel, S. C.; Chiang, M. Y.; Rauscher, D. J.; Buhro, W. E. *J. Am. Chem. Soc.* **1993**, *115*, 160.
- (8) Druckenbrodt, C.; du Mont, W.-W.; Ruthe, F.; Jones, P. G. *Z. Anorg. Allg. Chem.* **1998**, *624*, 590.
- (9) Yao, S.; Brym, M.; Merz, K.; Driess, M. *Organometallics* **2008**, *27*, 3601.
- (10) Rivard, E.; Sutton, A. D.; Fettingner, J. C.; Power, P. P. *Inorg. Chim. Acta* **2007**, *360*, 1278.
- (11) Arif, A. M.; Cowley, A. H.; Jones, R. A.; Power, J. M. *J. Chem. Soc., Chem. Commun.* **1986**, 1446.
- (12) Merrill, W. A.; Rivard, E.; DeRopp, J. S.; Wang, X.; Ellis, B. D.; Fettingner, J. C.; Wrackmeyer, B.; Power, P. P. *Inorg. Chem.* **2010**, *49*, 8481.
- (13) For examples, see: (a) Westerhausen, M.; Hausen, H.-D.; Schwarz, W. Z. *Anorg. Allg. Chem.* **1996**, *622*, 903. (b) Westerhausen, M.; Krofta, M.; Wiberg, N.; Nöth, H.; Pfitzner, A. *Z. Naturforsch., B* **1998**, *53*, 1489. (c) Westerhausen, M.; Hausen, H.-D.; Schwarz, W. Z. *Anorg. Allg. Chem.* **1995**, *621*, 877. (d) Westerhausen, M.; Krofta, M.; Schneiderbauer, S.; Piotrowski, H. *Z. Anorg. Allg. Chem.* **2005**, *631*, 1391. (e) Allan, R. E.; Beswick, M. A.; Cromhout, N. L.; Paver, M. A.; Raithby, P. R.; Trevithick, M.; Wright, D. S. *Chem. Commun.* **1996**, 1501. (f) Garcia, F.; Hahn, J. P.; McPartlin, M.; Pask, C. M.; Rothenberger, A.; Stead, M. L.; Wright, D. S. *Organometallics* **2006**, *25*, 3275.
- (14) (a) Martin, D.; Baceiredo, A.; Gornitzka, H.; Schoeller, W. W.; Bertrand, G. *Angew. Chem., Int. Ed.* **2005**, *44*, 1700. (b) Masuda, J. D.; Martin, D.; Lyon-Saunier, C.; Baceiredo, A.; Gornitzka, H.; Donnadiu, B.; Bertrand, G. *Chem.—Asian J.* **2007**, *2*, 178.
- (15) Izod, K.; McFarlane, W.; Allen, B.; Clegg, W.; Harrington, R. W. *Organometallics* **2005**, *24*, 2157.
- (16) Izod, K.; Stewart, J.; Clark, E. R.; McFarlane, W.; Allen, B.; Clegg, W.; Harrington, R. W. *Organometallics* **2009**, *28*, 3327.
- (17) Izod, K.; Stewart, J.; Clegg, W.; Harrington, R. W. *Organometallics* **2010**, *29*, 108.
- (18) Izod, K.; Stewart, J.; Clark, E. R.; Clegg, W.; Harrington, R. W. *Inorg. Chem.* **2010**, *49*, 4698.
- (19) Blair, S.; Izod, K.; Harrington, R. W.; Clegg, W. *Organometallics* **2003**, *22*, 302.
- (20) Cheng, F.; Dyke, J. M.; Ferrante, F.; Hector, A. L.; Levason, W.; Ried, G.; Webster, M.; Zhang, W. *Dalton Trans.* **2010**, 39, 847.
- (21) Borisove, I. V.; Eaborn, C.; Hill, M. S.; Khrustalev, V. N.; Kuznetskova, M. G.; Smith, J. D.; Ustynuk, Y. A.; Lunin, V. V.; Zemlyansky, N. N. *Organometallics* **2002**, *21*, 4005.
- (22) Hitchcock, P. B.; Lappert, M. F.; Samways, B. J.; Weinberg, E. L. *J. Chem. Soc., Chem. Commun.* **1983**, 1492.
- (23) (a) Becke, A. D. *J. Chem. Phys.* **1993**, *98*, 5648. (b) Stephens, P. J.; Devlin, F. J.; Chablowski, C. F.; Frisch, M. J. *J. Phys. Chem.* **1994**, *98*, 11623. (c) Hertwig, R. H.; Koch, W. *Chem. Phys. Lett.* **1997**, *268*, 345.
- (24) (a) Hay, P. J.; Wadt, W. R. *J. Chem. Phys.* **1985**, *82*, 270. (b) Wadt, W. R.; Hay, P. J. *J. Chem. Phys.* **1985**, *82*, 284. (c) Hay, P. J.; Wadt, W. R. *J. Chem. Phys.* **1985**, *82*, 299.
- (25) (a) Hariharan, P. C.; Pople, J. A. *Theor. Chim. Acta* **1973**, *28*, 213. (b) Francl, M. M.; Pietro, W. J.; Hehre, W. J.; Binkley, J. S.; Gordon, M. S.; DeFrees, D. J.; Pople, J. A. *J. Chem. Phys.* **1982**, *77*, 3654.

(26) Blair, S.; Izod, K.; Taylor, R.; Clegg, W. *J. Organomet. Chem.* **2002**, *656*, 43.

(27) For examples, see: (a) Kurz, S.; Oessen, H.; Sieler, J.; Hey-Hawkins, E. *Phosphorus, Sulfur Silicon Relat. Elem.* **1996**, *117*, 189. (b) Andrews, P. C.; King, S. J.; Raston, C. L.; Roberts, B. A. *Chem. Commun.* **1998**, 547. (c) Loss, S.; Widauer, C.; Grützmacher, H. *Angew. Chem., Int. Ed.* **1999**, *38*, 3329. (d) Balazs, G.; Breunig, H. J.; Lork, E.; Offermann, W. *Organometallics* **2001**, *20*, 2666.

(28) (a) *CrysAlisPro*; Oxford Diffraction Ltd: Oxford, U.K., 2008. (b) Sheldrick, G. M. *Acta Crystallogr., Sect. A* **2008**, *64*, 112.

(29) Allen, F. H. *Acta Crystallogr., Sect. B* **2002**, *58*, 380.

(30) Frisch, M. J.; Trucks, G. W.; Schlegel, H. B.; Scuseria, G. E.; Robb, M. A.; Cheeseman, J. R.; Montgomery, Jr., J. A.; Vreven, T.; Kudin, K. N.; Burant, J. C.; Millam, J. M.; Iyengar, S. S.; Tomasi, J.; Barone, V.; Mennucci, B.; Cossi, M.; Scalmani, G.; Rega, N.; Petersson, G. A.; Nakatsuji, H.; Hada, M.; Ehara, M.; Toyota, K.; Fukuda, R.; Hasegawa, J.; Ishida, M.; Nakajima, T.; Honda, Y.; Kitao, O.; Nakai, H.; Klene, M.; Li, X.; Knox, J. E.; Hratchian, H. P.; Cross, J. B.; Bakken, V.; Adamo, C.; Jaramillo, J.; Gomperts, R.; Stratmann, R. E.; Yazyev, O.; Austin, A. J.; Cammi, R.; Pomelli, C.; Ochterski, J. W.; Ayala, P. Y.; Morokuma, K.; Voth, G. A.; Salvador, P.; Dannenberg, J. J.; Zakrzewski, V. G.; Dapprich, S.; Daniels, A. D.; Strain, M. C.; Farkas, O.; Malick, D. K.; Rabuck, A. D.; Raghavachari, K.; Foresman, J. B.; Ortiz, J. V.; Cui, Q.; Baboul, A. G.; Clifford, S.; Cioslowski, J.; Stefanov, B. B.; Liu, G.; Liashenko, A.; Piskorz, P.; Komaromi, I.; Martin, R. L.; Fox, D. J.; Keith, T.; Al-Laham, M. A.; Peng, C. Y.; Nanayakkara, A.; Challacombe, M.; Gill, P. M. W.; Johnson, B.; Chen, W.; Wong, M. W.; Gonzalez, C.; Pople, J. A. *Gaussian 03*, revision D.01; Gaussian, Inc.: Wallingford, CT, 2004.